ADVANCED FUNCTIONAL MATERIALS

Supporting Information

for *Adv. Funct. Mater.,* DOI: 10.1002/adfm.202212093

Bio-Inspired Semi-Active Safeguarding Design with Enhanced Impact Resistance via Shape Memory Effect

Wenhui Wang, Sheng Wang, Jianyu Zhou, Huaxia Deng, Shuaishuai Sun, Tian Xue, Yuqian Ma,* and Xinglong Gong**

Supporting Information

Bio-inspired Semi-active Safeguarding Design with Enhanced Impact Resistance via Shape Memory Effect

Wenhui Wang, Sheng Wang, Jianyu Zhou, Huaxia Deng, Shuaishuai Sun, Tian Xue, Yuqian Ma* and Xinglong Gong**

This file includes:

1. Experimental section

1.1. Materials

Hydroxyl silicone oil, boric acid, and benzoyl peroxide (BPO) were supplied by Sinopharm Chemical Reagent Co. Ltd. (China). Methyl vinyl silicone rubber (VMQ) was purchased from Shenzhen Muwei Technology Co., Ltd. (China). Polycaprolactone (PCL) was provided by Yuancheng Plastic & Chemical Co., Ltd. (China). The 0.01 mm metal film with the main component of iron-chromium-aluminum was bought from Jiangsu Shuohao Electric Heating Co., Ltd. (China). Kapton film was obtained from Hangzhou Ubisheng flagship store (China). Ethylene Vinyl Acetate foam (EVA) was bought from Shenzhen Mileqi Tape Co., Ltd. (China). Silicone rubber was purchased from JianWei (J&V) Technology Co., Ltd. (China). PDMS prepolymer and curing agent (Sylgard 184) were supplied by Dow Corning GmbH (Germany). All chemical reagents were purchased from commercial sources and used without further purification.

1.2. Preparation procedures

Preparation of SSG: Briefly, boric acid was added into hydroxyl silicone oil with a mass ratio of 1:36. The mixture solution was heated at 180 °C for 2 hours. During the process, octanoic acid was also thoroughly mixed. After cooling to room temperature, the shear stiffening gel (SSG) was obtained, where dynamic coordination bonds between B and O elements in the Si-O groups, and entanglements were formed.

Preparation of SSE and PCLE: Firstly, 21 g SSG and 9 g VMQ were mixed by a double-roll mill (Taihu Rubber Machinery Inc., China, Model XK-160). BPO was added as the vulcanized agent. Subsequently, PCL was also mixed into the composites at different mass fractions. The final material was pressed into a mold and vulcanized to obtain the PCLE. PCLE was cut to desired shape for applications. The fabrication process of PCLE was presented in **Scheme S1.** When the mass ratio of PCL was X%, the composite was denoted as PCLE-X%. PCLE-0% (also named SSE), PCLE-20%, PCLE-30%, PCLE-40%, and PCLE-50% were prepared and measured in detail, because PCLE-60% exhibited low fracture strain. However, PCL and SSE could not uniformly mix together when PCL content increased to 70%.

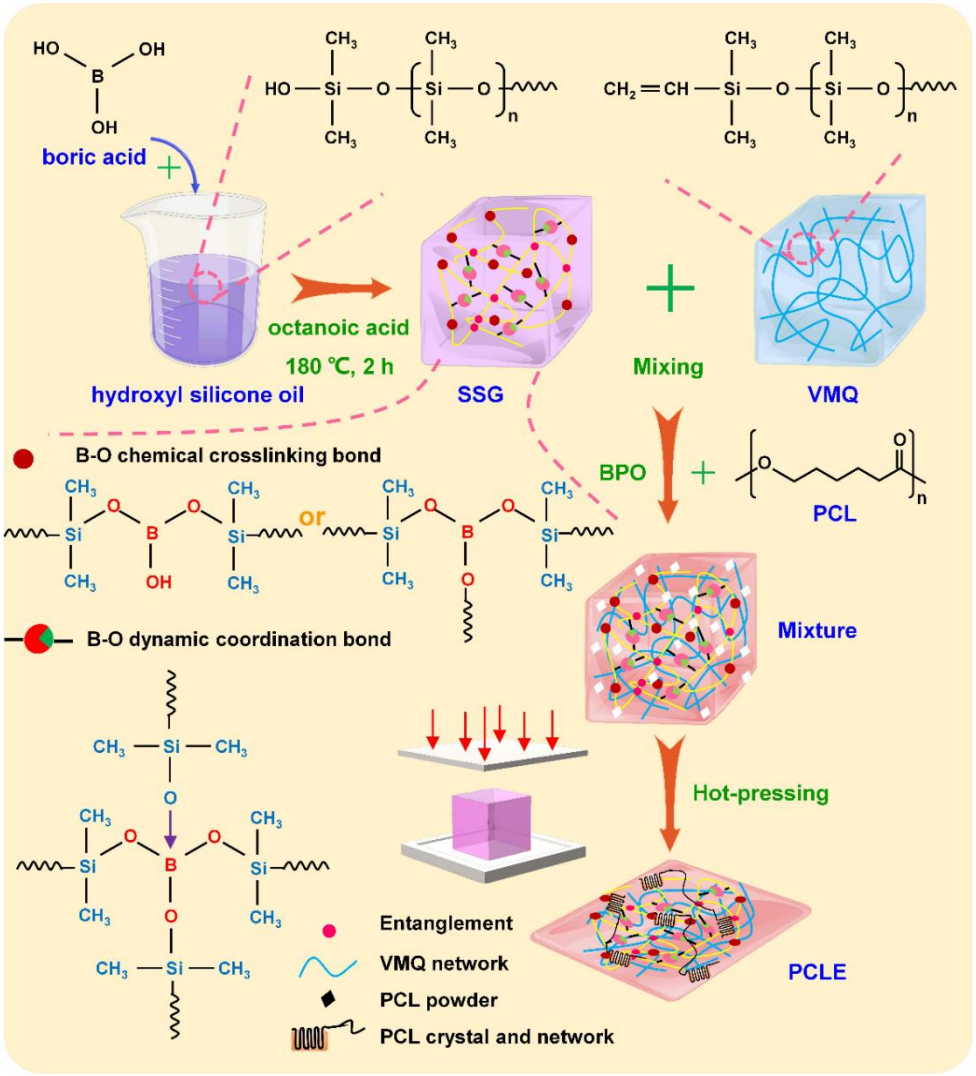

Scheme S1. The fabrication process of PCLE.

The fabrication procedures of ASPE and AMPE: Initially, PCLE-50% was heated above the transition temperature (T_t), followed by stretching to a certain strain. Keeping loading, the PCLE-50% was cooled to room temperature. Ultimately, the trimmed metal film was attached to the surface of the shape-programmed PCLE-50% and encapsulated with Kapton tape to obtain the assembled single-branch structure PCLE (ASPE). The assembled multi-branch structure PCLE (AMPE) was prepared from multiple ASPEs. AMPE-x indicated that AMPE consists of x ASPEs.

1.3. Characterization

1.3.1 Differential scanning calorimetry (DSC)

The DSC was conducted using TA DSC-Q2000 to evaluate the T_t of PCLE. Each sample was heated from -90 ℃ to 90 ℃ at 10 ℃ min^{-1}, kept at 90 ℃ for 5 min, and then cooled at the same rate. And it was heated again from -90 ℃ to 90 ℃ at 10 ℃ min^{-1}.

1.3.2 Uniaxial tension test

The uniaxial tension test was performed on an MTS Universal Materials Testing Machine (Criterion Model 43) at room temperature. The composites with the dimension of 25 mm × 10 mm × 2 mm were stretched at different rates from 0.01 s^{-1} to 0.20 s^{-1}.

1.3.3 Rheological behavior test

The storage modulus and loss factors of PCLE were measured using a commercial rheometer (Physica MCR 302, Anton Paar Co., Austria). The composites, molded into a cylinder shape with a thickness of 1 mm and diameter of 20 mm, were tested with a parallel plate under oscillatory shear.

1.3.4 Thermal gravimetric analysis (TGA)

The thermal stability of PCLE was investigated by a thermogravimetric analyzer (TGA Q5000IR, USA) from 30 ℃ to 800 ℃ at a heating rate of 10 ℃ min^{-1} under nitrogen gas conditions.

1.3.5 Dynamic mechanical analysis (DMA)

DMA was conducted on a Q800 (TA instrument) tester with a tensile clamp in a "Multi-Frequency-Strain" mode with a frequency of 1 Hz. The test was performed using the heating rate of 5 °C min^{-1} from -90 °C to 90 °C under an air atmosphere.

1.3.6 Scanning electron microscopy (SEM)

The morphological structures of PCL, SSE, and PCLE-50% were characterized by field emission scanning electron microscopy (SEM, Gemini 500, Carl Zeiss Jena, Germany) at an acceleration voltage of 3 kV.

1.3.7 Shape memory test

Heating by hot water, hot air, or Joule-heat was employed to elevate composites' temperature and stimulate the shape memory effect. To evaluate the shape memory behavior, the PCLEs with different PCL contents were cut into cuboids and subjected to the following deformation and recovery programs. The specimen (80 mm × 15 mm × 2 mm) was immersed in a water bath at 65 ℃ for 1 min. Subsequently, it was deformed into a temporary shape (length of 120 mm). With the deformation maintained, it was cooled to room temperature. The shape-fixing state was completed after unloading. Finally, its shape recovery was accomplished by immersing the deformed PCLE in the same bath at 60 ℃.

Particularly, thermodynamic curves of PCLE-50% under different tensile strains were carried out using a DMA Q800 under a "strain rate" mode. Briefly, a rectangular specimen with a dimension of 10 mm × 5 mm × 2 mm was deformed at 60 °C with 20% min^{-1} followed by an isothermal hold for 10 min. It was cooled to 25 °C at 5 °C min^{-1} while holding constant

tensile strain. The force was unloaded and kept isothermal for another 10 min to finish the shape fixing process. The composite was heated to 60 °C at 5 °C min^{-1} for triggering shape recovery.

The shape fixity ratio (R_f) and shape recovery ratio (R_r) were respectively calculated using the following equations:

$$R_f = \frac{\varepsilon}{\varepsilon_{load}} \times 100\% \quad (1)$$

$$R_f = \frac{\varepsilon - \varepsilon_{rec}}{\varepsilon} \times 100\% \quad (2)$$

where ε_{load}, ε, and ε_{rec} represented the strain before unloading, after unloading, and after recovery, respectively.

1.3.8 Drop hammer test

The anti-impact performance of the specimens was investigated by a drop hammer test system including a drop hammer device, charge amplifier, and oscilloscope. During the experiment, the impactor dropped freely from different heights followed by recording the force and acceleration signals. In this work, two impactors were used. Type-A was the rounded impactor with a mass of 0.54 kg and a diameter of 20 mm. Type-B was the flat impactor with a mass of 0.57 kg and a diameter of 90 mm.

Moreover, the hammer was assumed to free-fall without any frictional resistance. According to energy conversation law, the initial kinetic energy (E_0) and initial velocity (v_0) of hammer at impact moment (t_0) were obtained as follows:

$$E_0 = mgh, \ v_0 = \sqrt{2gh} \quad (3)$$

where m and g were the mass of hammer (0.57 kg) and gravity acceleration (9.8 m s^{-2}) respectively. The velocity (v_1) of hammer at rebound moment (t_1) was as follow:

$$v_1 = v_0 - \int a\,dt = \sqrt{2gh} - \int_{t_0}^{t_1} a\,dt \quad (4)$$

in which the second term denoted as the integral of acceleration (a) over entire impact-rebound time, which is greater than v_0, because v_1 is negative in the opposite direction of v_0 (Inset in Figure 4h). Thus the energy absorption (ΔE) during impact process could be calculated as follow:

$$\Delta E = E_0 - \frac{1}{2}mv_1^2 = mgh - \frac{1}{2}m(\sqrt{2gh} - \int_{t_0}^{t_1} a\,dt)^2 \quad (5)$$

1.3.9 Infrared temperature measurement

Thermal images were all collected by an Infrared camera (Image IR 8300, InfraTec, Germany).

1.3.10 Thermal conductivity measurement

Thermal conductivity was measured by a Thermal Constants Analyzer (Hot Disk TPS 2500 S).

2. Simulation section

In this work, a finite element analysis (FEA) was developed to evaluate the shape memory and recovery behavior of PCLE. Many modeling studies have been performed,[1-3] and two approaches have generally been employed based on different constitutive formulations. The first modeling approach treated the material as a biphasic system consisting of glassy and rubbery phases. It was used to predict temperature-dependent behavior, but not rate-dependent behavior. The second modeling method utilized the viscoelastic properties of the SMP obtained via rheology or dynamic mechanical analysis to model time- and temperature- dependent recovery behavior. Here, the second approach was employed.

Firstly, the time and temperature dependent shear modulus was measured by the rheometer. PCLE-50% was subjected to an oscillatory strain of 0.1% across a frequency sweep from 0.1 Hz to 100 Hz. This frequency sweep was repeated at 5 ℃ increments ranging from 25 ℃ to 65 ℃. The material shear storage modulus (*G'*) and loss factor (*tan δ*) were shown in **Figure I**, respectively.

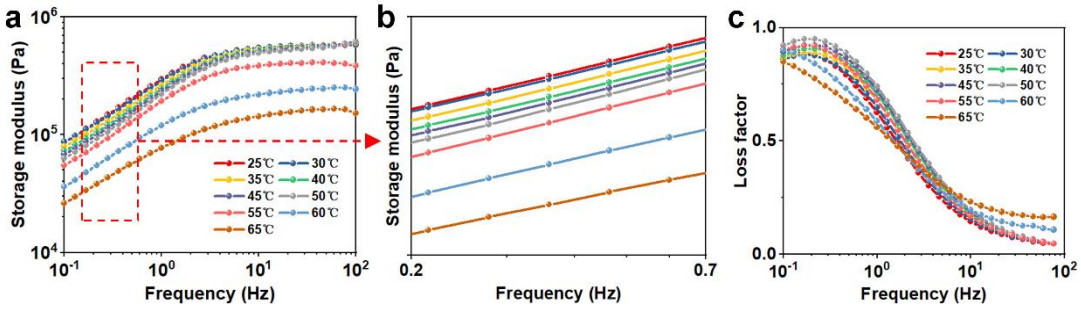

Figure I. (a, b) The storage modulus and (c) loss factor of PCLE-50% at different temperatures.

Thus, the influence of temperature on the viscoelastic behavior of SMP was especially important. The material was assumed to be thermo-rheological simple (all relaxation times were affected by temperature in the same way), and isothermal frequency sweep data was shifted horizontally in frequency according to the Time-Temperature Superposition Principle (TTSP) using the Williams-Landel-Ferry (WLF) equation:

$$\log(a_t) = -\frac{C_1(T-T_{ref})}{C_2+(T-T_{ref})}$$

(6)

where a_t was the shift factor for the time and temperature dependent properties, C_1 and C_2 were empirical parameters, T represented the experimental temperature, and T_{ref} indicated the reference temperature. The viscoelastic master curves at the reference temperature (T_{ref} = 55 ℃) were obtained with the values of C_1 = 8.86 and C_2 = 101.6 (**Figure II**).

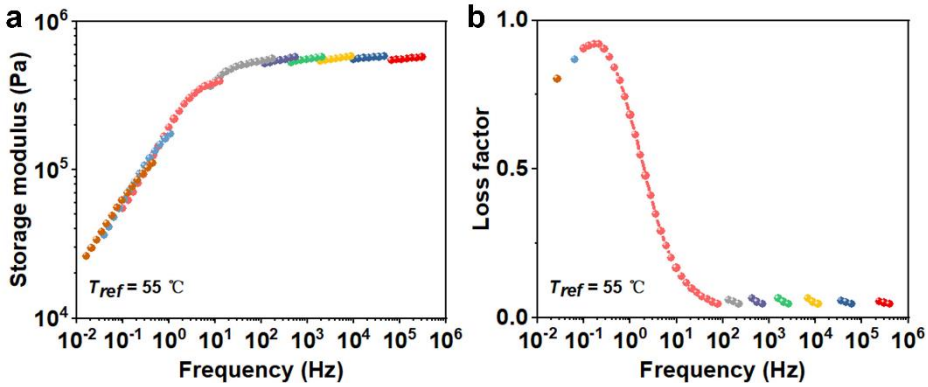

Figure II. The master-curves of (a) storage modulus and (b) loss factor shifted to a reference temperature of T_{ref} = 55 ℃.

Then, these curves were fitted using a Prony series to represent a generalized Maxwell model (**Figure III**). The Prony series for the storage and loss moduli of a viscoelastic material could be implemented in Abaqus according to:

$$G'(f) = G_0[1 - \sum_{i=1}^{n} g_i] + G_0 \sum_{i=1}^{n} \frac{g_i(2\pi f\tau_i)^2}{1+(2\pi f\tau_i)^2}$$

(7)

$$G''(f) = G_0 \sum_{i=1}^{n} \frac{g_i(2\pi f\tau_i)}{1+(2\pi f\tau_i)^2}$$

(8)

$$tan\,\delta = \frac{G''(f)}{G'(f)}$$

(9)

in which G_0 represented the instantaneous shear modulus and f indicated the frequency in Hz. The g_i were a series of suitable dimensionless relaxation moduli and τ_i were relaxation times. The calculated Prony series coefficients were summarized in **Table I**. Other material properties used as inputs to the finite element model were listed in **Table II**. Four General-Visco steps were set in the model, namely ‘high temp load’, ‘down temp’, ‘unload’ and ‘up temp’, corresponding to the four processes of shape programming, cooling down, unloading and shape recovery. The geometric nonlinearity was turned on.

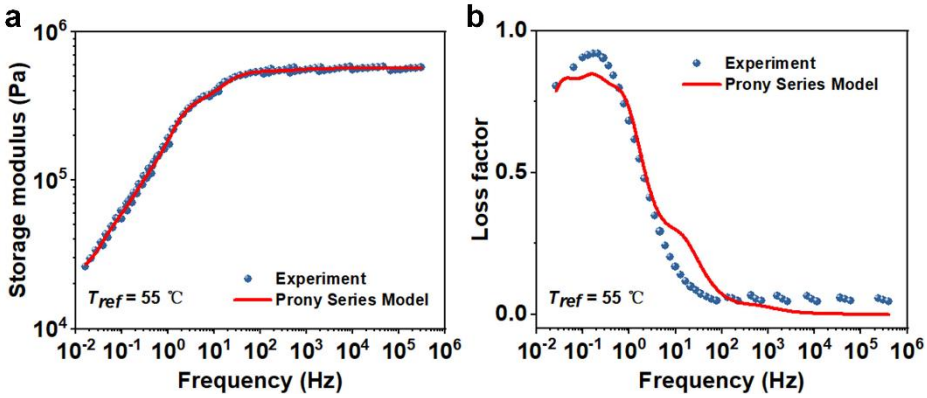

Figure III. The fitted master-curves of (a) storage modulus and (b) loss factor with Prony series at T_{ref} = 55 ℃.

Table I Prony series coefficients

#	1	2	3	4	5	6
g_i	0.04017	0.16701	0.16749	0.41931	0.10773	0.05762
τ_i (s)	2.37181E-4	0.00911	0.00911	0.10586	0.65787	3.60409

Table II Material properties used in the finite element model

Mass density	960 kg m^{-3}
Thermal Expansion	4.37×10^{-4} $℃^{-1}$ (T < 55℃) 2.25×10^{-4} $℃^{-1}$ (T≥55℃)
WLF Parameters	C_1 = 8.86 C_2 = 101.6 T_g = 55 ℃
Hyper-elastic for Neo Hooke	*C10*=210000 *D1*=4.6e-6 Moduli time scale: Instantaneous

The simplified finite element models were further established to simulate the deformation process of the double-layer structure before and after the shape change resisting the impact of 300 mm drop hammer. The hammer and substrate were regarded as rigid body constraints and their deformation was not considered. The hammer impacted at an initial velocity (v_0) of 2.42 m/s and the base was fixed **(Figure IV)**. The Dynamic Explicit step was used.

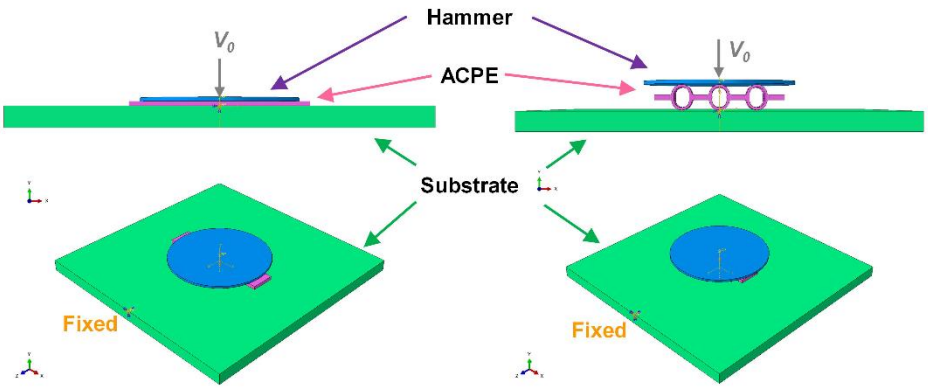

Figure IV. Impact models and their boundary conditions.

[1] T. Liu, L. Liu, C. Zeng, Y. Liu, J. Leng, 4D printed anisotropic structures with tailored mechanical behaviors and shape memory effects. *Compos. Sci. Technol*. **2020**, 186, 107935.
[2] R. Mailen, Y. Liu, M. Dickey, M. Zikry, J. Genzer, Modelling of shape memory polymer sheets that self-fold in response to localized heating. *Soft Matter*. **2015**, 11, 7827.
[3] L. Zhang, H. Du, L. Liu, Y. Liu, J. Leng, Analysis and design of smart mandrels using shape memory polymers. *Compos. B. Eng.* **2014**, 59, 230-237.

3. Figures

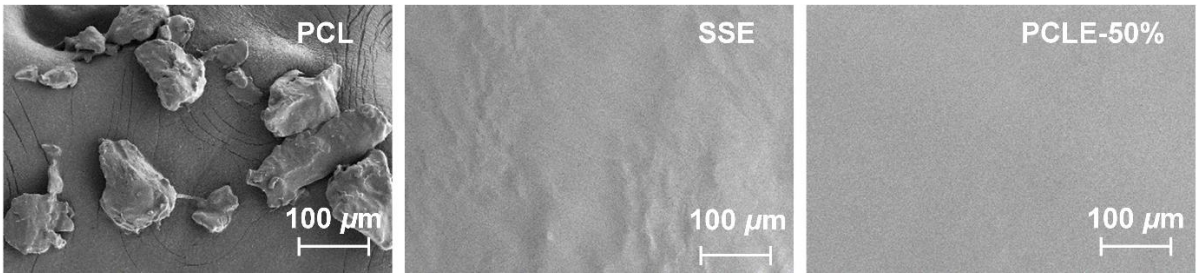

Figure S1. SEM images of the PCL, SSE, and PCLE-50%.

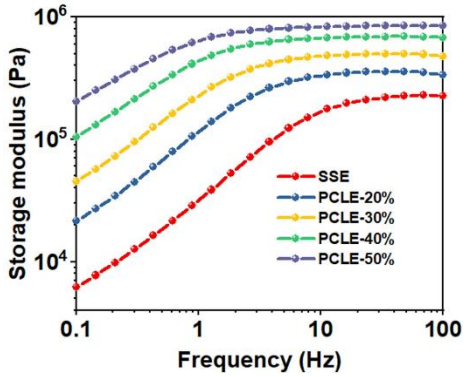

Figure S2. Storage modulus of PCLE when the shear frequency varied from 0.1 H to 100 Hz.

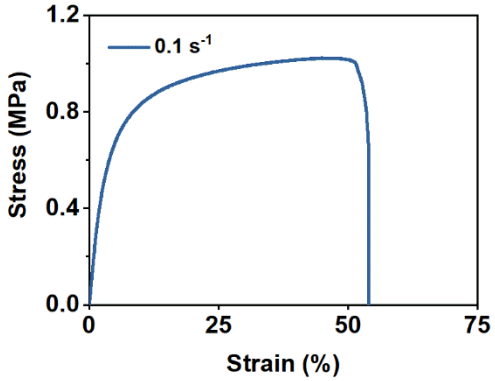

Figure S3. The stress-strain curve of PCLE-60% at strain rate of 0.1 s^{-1}.

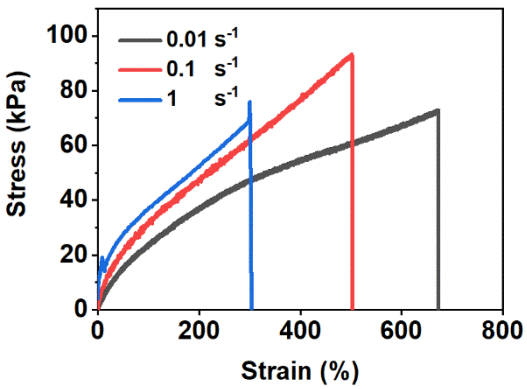

Figure S4. Stress-strain curves of SSE at different tensile strain rates.

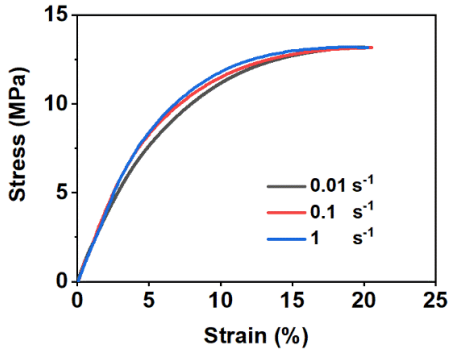

Figure S5. Stress-strain curves of PCL at different tensile strain rates.

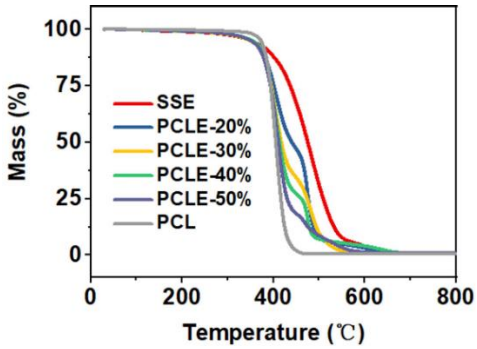

Figure S6. TGA of PCLE.

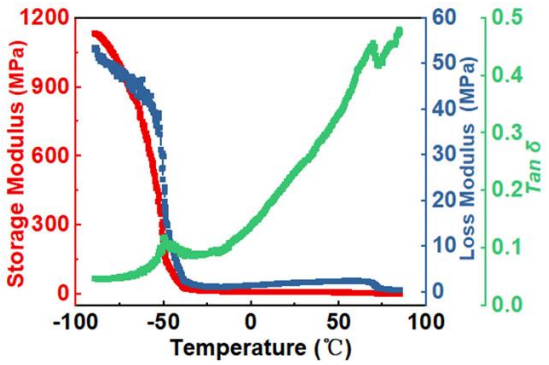

Figure S7. Storage modulus, loss modulus, and tan δ of PCLE-50% as a function of temperature tested by DMA Q800.

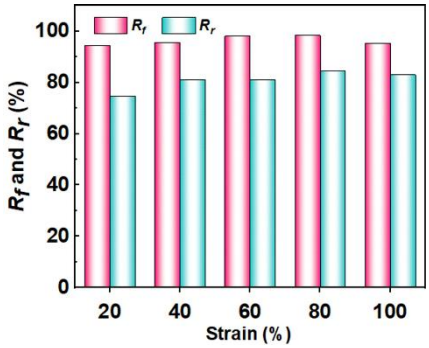

Figure S8. R_f and R_r of PCLE-50% were calculated from thermal-mechanical curves.

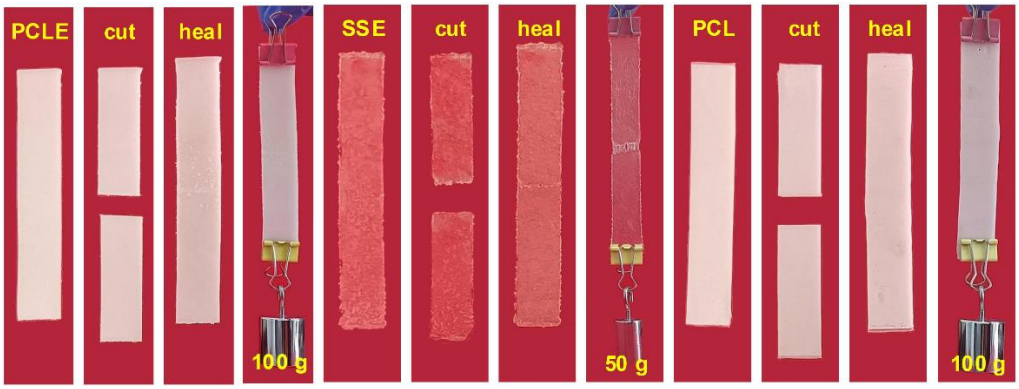

Figure S9. Self-healing properties of PCLE-50%, SSE, and PCL.

Figure S10. The shape recovery processes of PCLE-50% when heated by hot water of 60 ℃.

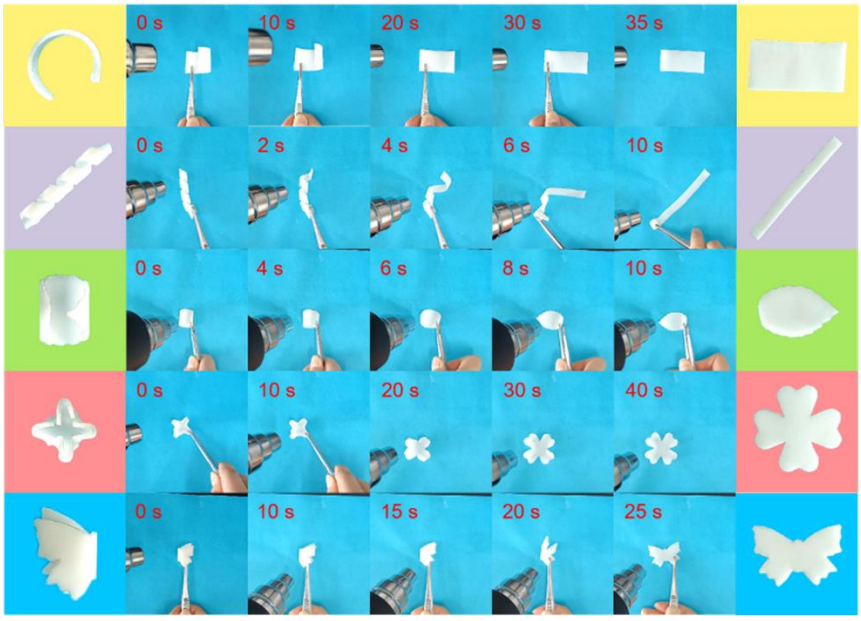

Figure S11. The shape recovery processes of PCLE-50% when heated by hot air of 100 ℃.

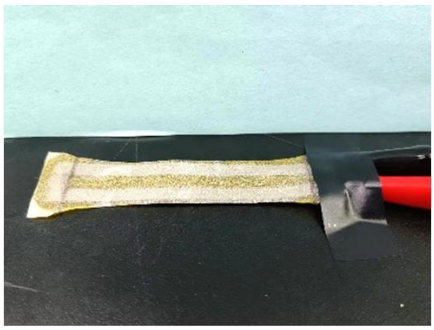

Figure S12. Specimen without pre-tension programming did not bend after heating, excluding the influence of differences in thermal expansion coefficients of materials.

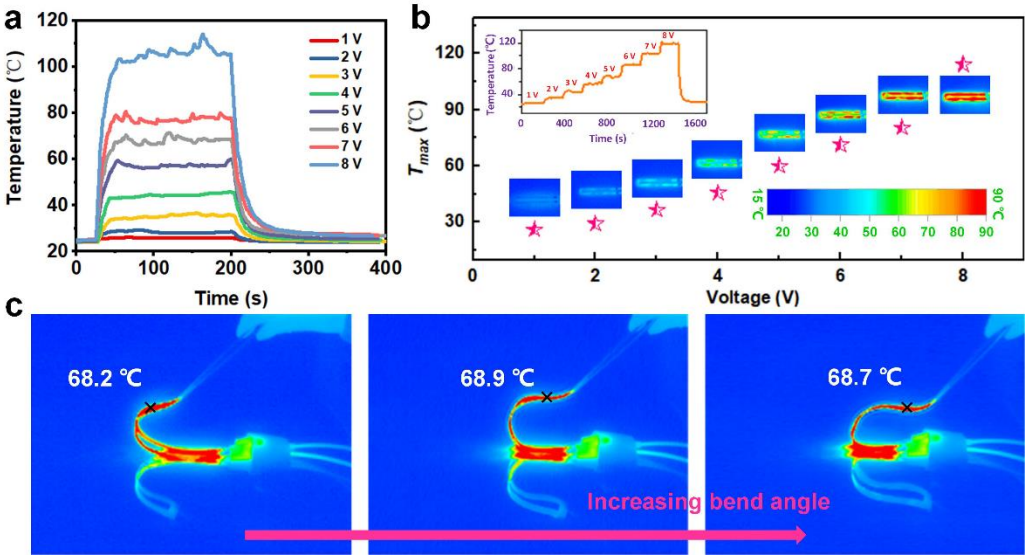

Figure S13. Electro-thermal properties of the metal films. (a) Time-dependent temperatures of the metal film at applied voltages of 1 V to 8 V. (b) The maximum temperatures (T_{max}) and their infrared temperature photos at applied voltages of 1 V to 8 V. The inset showed the stepped heating temperature curve. (c) Infrared temperature photos of the metal film at different bending angles when the voltage was 6 V.

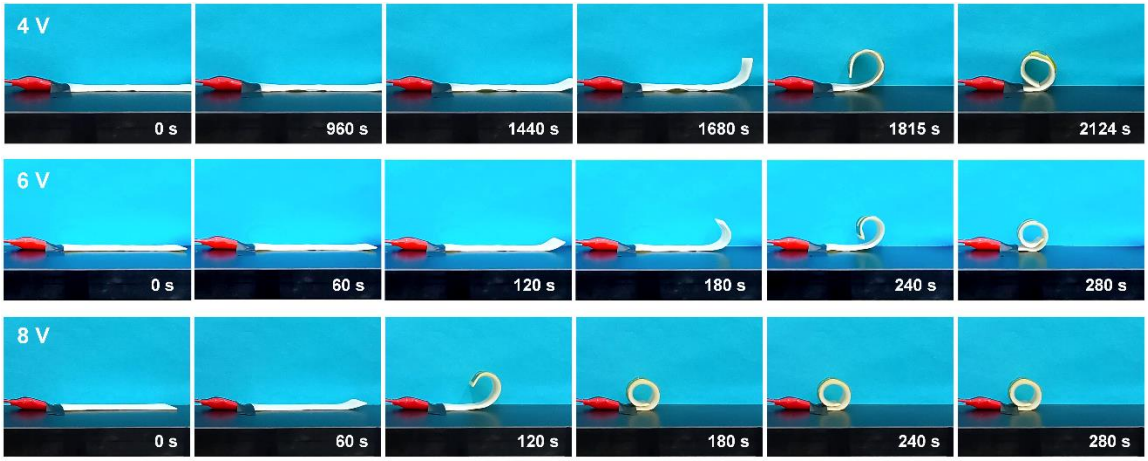

Figure S14. The deformation processes of ASPE with pretension strain of 50% at heating voltage of 4V, 6 V and 8V.

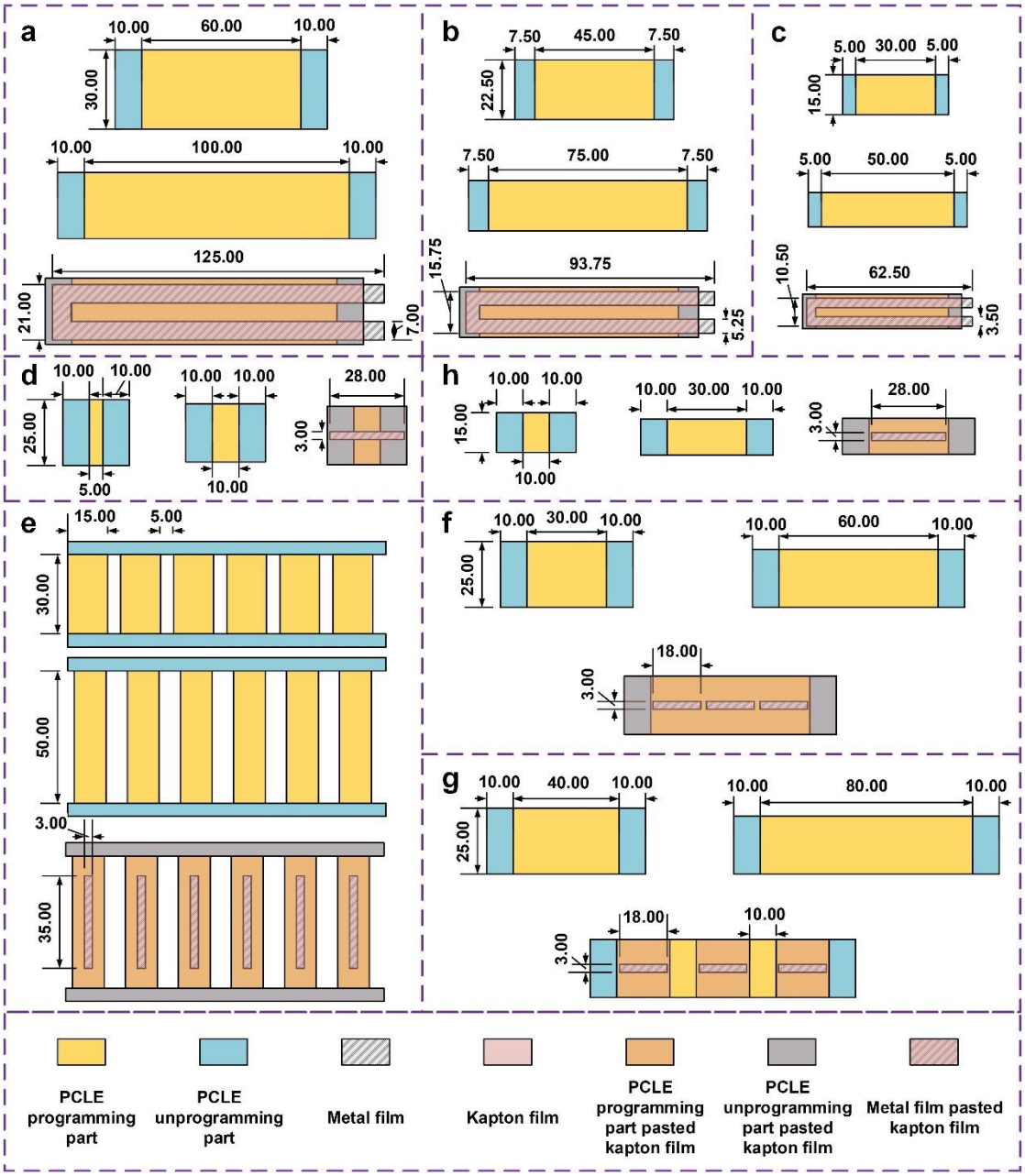

Figure S15. Dimensional drawings of different structures in this work. (a) ASPE with a size ratio of 1.00. (b) ASPE with a size ratio of 0.75 and also used to obtain AMPE. (c) ASPE with a size ratio of 0.50. (d) The square structures, triangular structure, rectangular structure, and hexagonal structure. (e) The grid structure. (f) The single-layer structure. (g) The double-layer structure. (h) Other shape deformation structures in decorative clothing.

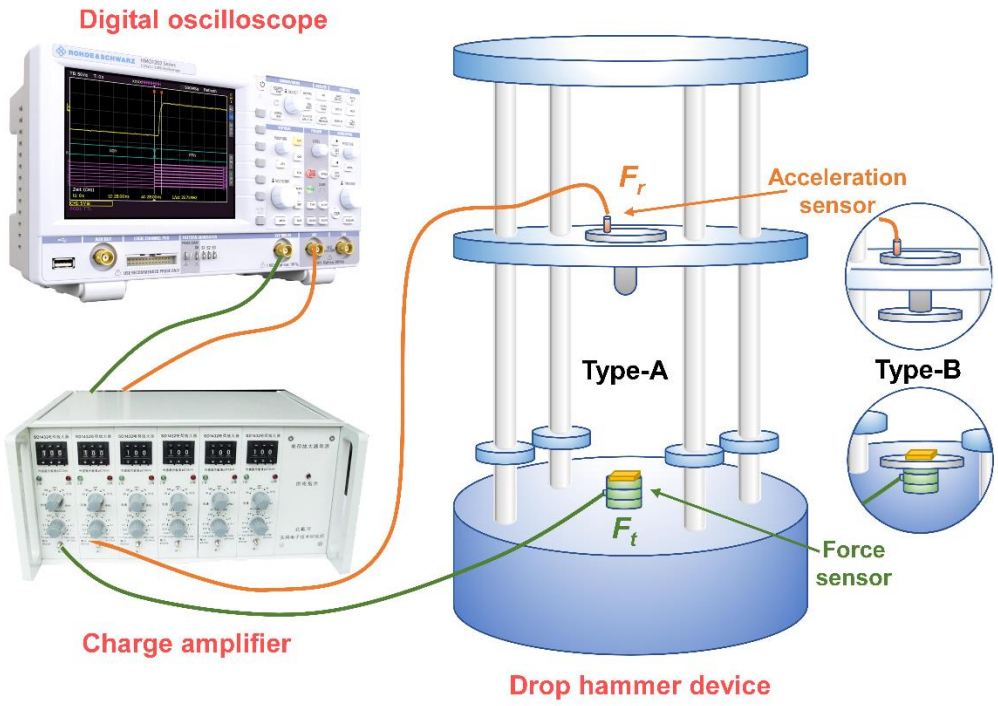

Figure S16. Drop hammer test system included a drop hammer device, charge amplifier, and oscilloscope. Type-A was the rounded impactor with a mass of 0.54 kg and a diameter of 20 mm. Type-B was the flat impactor with a mass of 0.57 kg and a diameter of 90 mm.

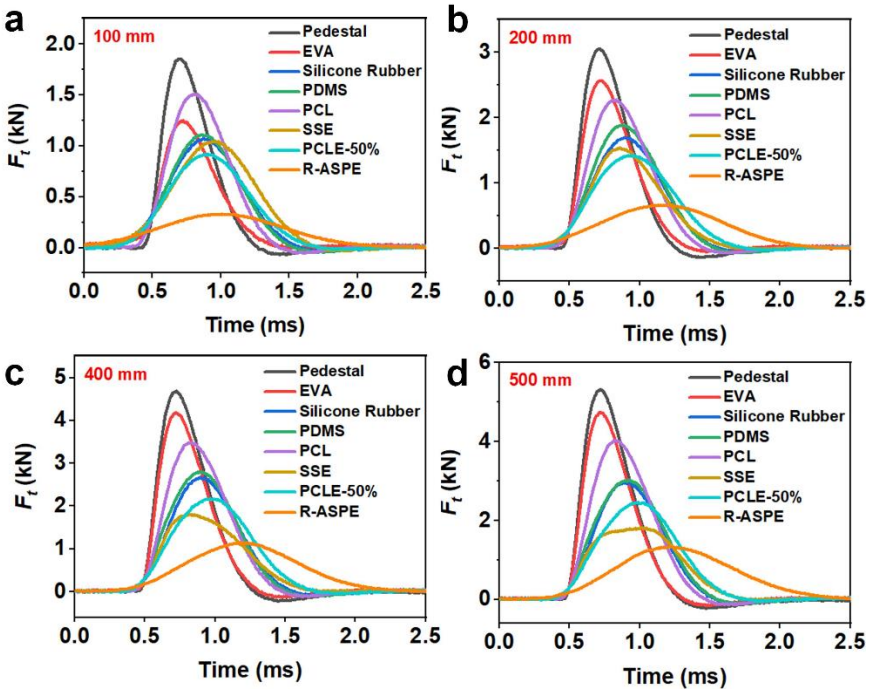

Figure S17. The impact forces of different materials when the drop hammer height of (a) 100 mm, (b) 200 mm, (c) 400 mm and (d) 500 mm.

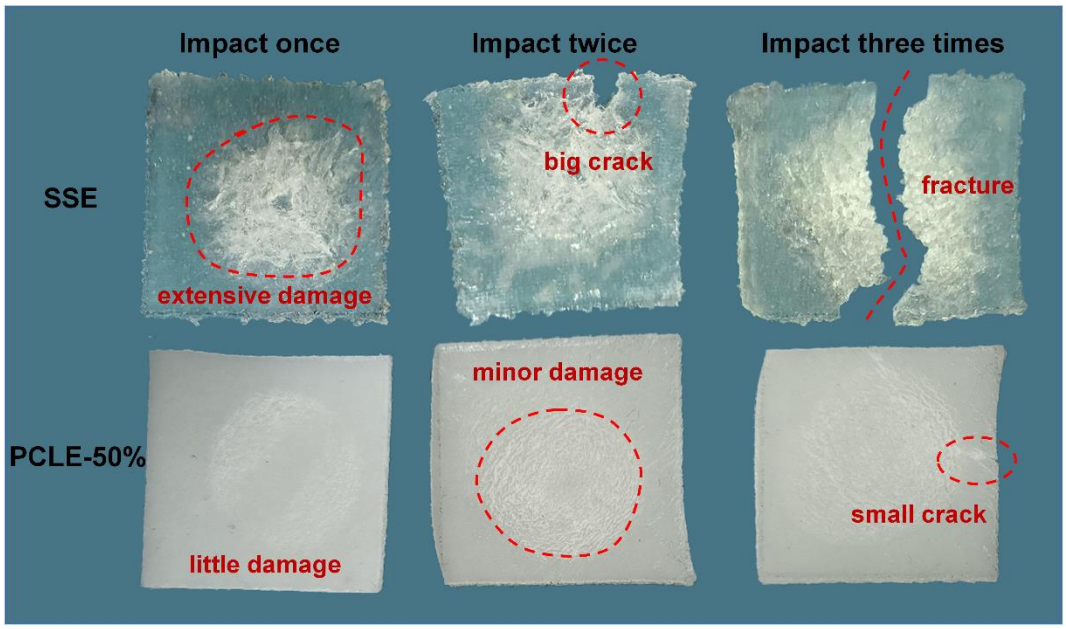

Figure S18. Photographs of SSE and PCLE-50% after three impacts.

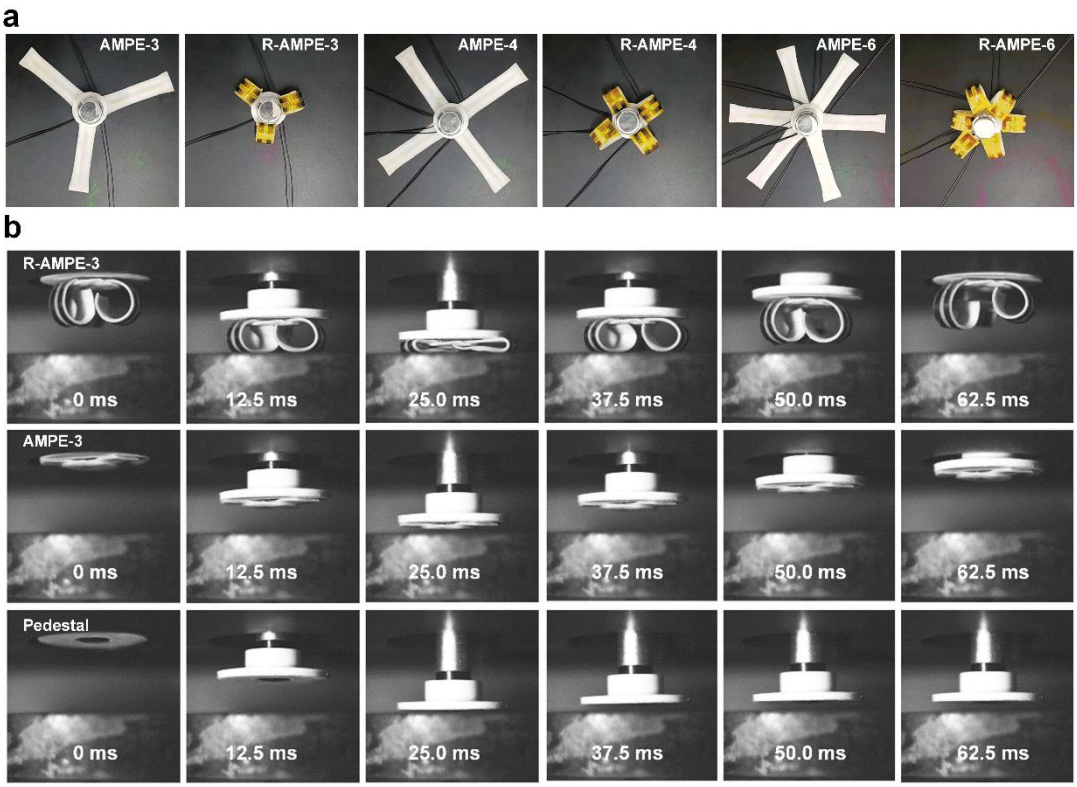

Figure S19. (a) The photos before and after AMPE structural change. (b) High-speed photographs of R-AMPE-3, AMPE-3, and pedestal during the 300 mm drop hammer impact processes.

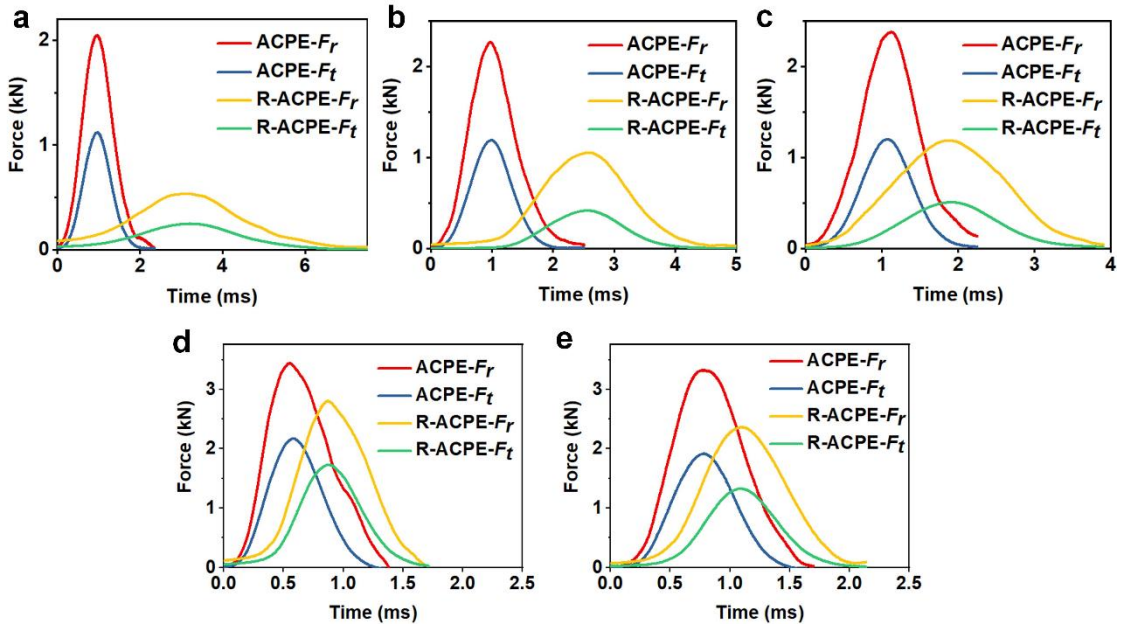

Figure S20. The forces of (a) triangular structure, (b) rectangular structure, (c) hexagonal structure, (d) single-layer structure, and (e) double-layer structure from a 300 mm drop hammer impact.

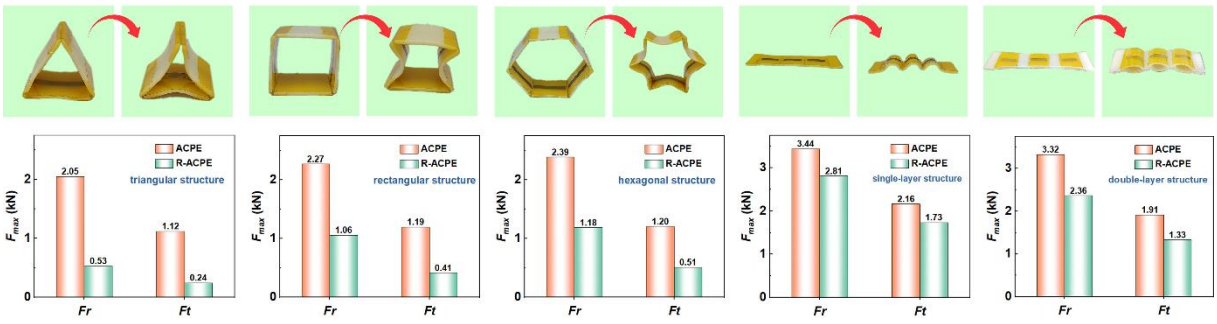

Figure S21. The maximum impact forces of triangular structure, rectangular structure, hexagonal structure, single-layer structure, and double-layer structure during the 300 mm drop hammer impact.

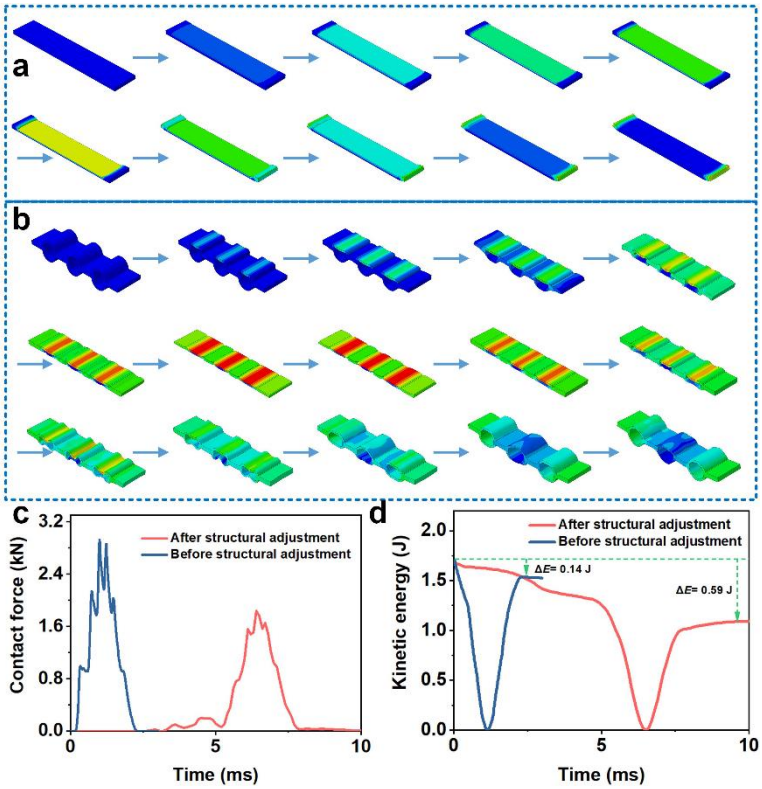

Figure S22. The simulation results of the double-layer structure resisting impact. Deformation displacement of the double-layer structure (a) before and (b) after structural adjustment during resisting the 300 mm drop hammer impact. (c) The contact force between the ACPE and substrate. (d) The kinetic energy of the hammer.

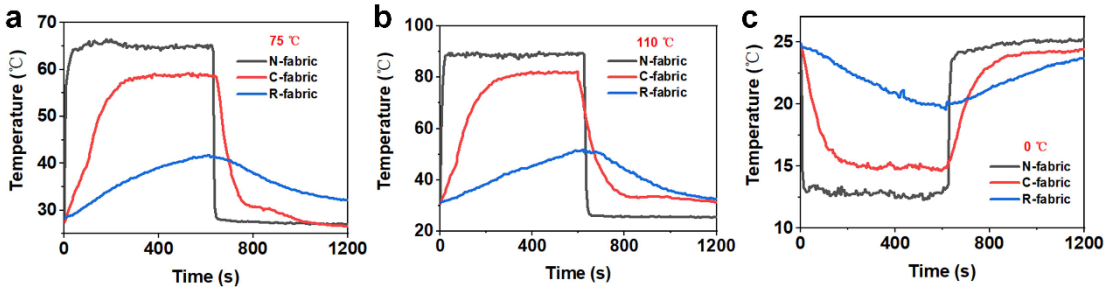

Figure S23. The center point infrared temperatures of the upper surface for different fabrics when the contact temperature of the bottom surface was (a) 75 ℃, (b) 110 ℃, and (c) 0 ℃.

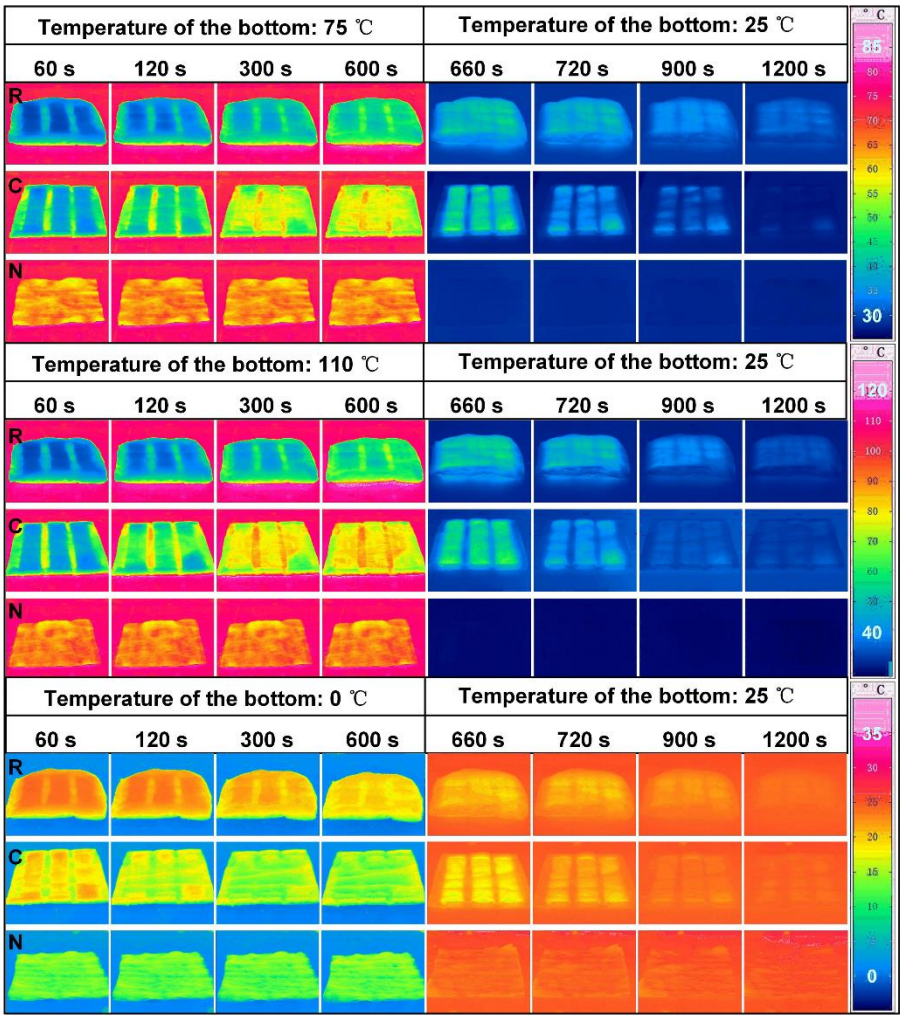

Figure S24. The upper surface infrared images of different fabrics when the contact temperature of the bottom surface was (a) 75 ℃, (b) 110 ℃, and (c) 0 ℃.

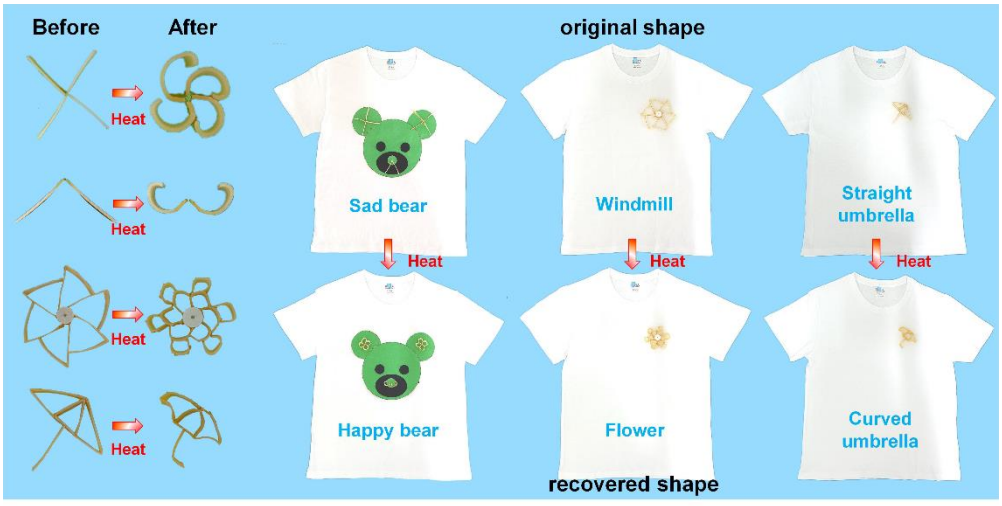

Figure S25. Intelligent decorative clothing.

Figure S26. The photos of the man wearing the different shape deformations decorative clothing.